

Article

Recycled Construction and Demolition Waste as Supplementary Cementing Materials in Eco-Friendly Concrete

Silvina V. Zito ^{*}, Edgardo F. Irassar  and Viviana F. Rahhal

Facultad de Ingeniería, CIFICEN (UNCPBA-CICPBA-CONICET), Olavarría B7400JWI, Argentina; firassar@fio.unicen.edu.ar (E.F.I.); vrahhal@fio.unicen.edu.ar (V.F.R.)

* Correspondence: silvina.zito@gmail.com

Abstract: Growing environmental awareness and scarcity of natural resources are forcing the world to migrate from linear to circular economies. The possibility of partially replacing cement with ceramic-based waste from construction and demolition waste (C&DW) is a government and industry focus. The present study analyzes the effects of including finely ground complete walls of ceramic blocks (including masonry mortars) as supplementary cementing materials (SCM) on the physical, mechanical, and transport properties (water absorption and permeability) of concrete. The replacement ratio employed was 25% by weight of cement. Studies of the hydration evolution of cement pastes support the described properties of concretes. The findings reveal that the ground ceramic-based waste from C&DW stimulates hydration at all ages. Initially, this stimulation is predominantly physical (filler effect), but in later stages, it becomes chemical (pozzolanic reaction). Based on the results obtained in this study, it is possible to produce concrete with mechanical properties comparable to those of conventional concrete at 28 days.

Keywords: C&DW; SCM; concrete



Citation: Zito, S.V.; Irassar, E.F.; Rahhal, V.F. Recycled Construction and Demolition Waste as Supplementary Cementing Materials in Eco-Friendly Concrete. *Recycling* **2023**, *8*, 54. <https://doi.org/10.3390/recycling8040054>

Academic Editor: Abdol R. Chini

Received: 30 March 2023

Revised: 18 June 2023

Accepted: 26 June 2023

Published: 28 June 2023



Copyright: © 2023 by the authors. Licensee MDPI, Basel, Switzerland. This article is an open access article distributed under the terms and conditions of the Creative Commons Attribution (CC BY) license (<https://creativecommons.org/licenses/by/4.0/>).

1. Introduction

In recent decades, there has been growth in the construction industry due to the development of a modern society, which demands new and better infrastructure, housing, and services [1]. However, although this sector's contributes to gross domestic product and employment generation, it also contributes to environmental degradation [2]. According to a report by the Organization for Economic Cooperation and Development (OECD), the construction sector is responsible for approximately 30% of raw material consumption, 42% of energy consumption, 12% of land use, 40% of atmospheric emissions, 20% of liquid effluents, 35% of total solid waste, and 13% of other emissions [3,4].

Construction and demolition waste (C&DW) refers to the solid waste generated from construction sites and the total or partial demolition of buildings and infrastructures. Construction waste often arises from the excessive ordering of supplies or mishandling of materials, while demolition involves the removal of outdated and unusable structures to make way for new structures. Additionally, CD&W can be generated after natural disasters [5]. Unfortunately, C&DW is often disposed through dumping and landfilling, leading to various social and environmental issues, such as safety hazards and contamination of soil and water sources [6,7].

The composition of the C&DW can vary depending on the construction system employed in each country; however, it, generally, it consists of concrete, ceramics, glass, steel, plastic, and wood; concrete and ceramic wastes (CW) accounts for more than 80% of this waste [8].

To address these challenges, recycling technologies for C&DW have been developed, and concrete and CW are increasingly recycled and used to produce recycled aggregate concrete [9–11]. The properties of concrete with recycled concrete aggregate are similar to

those with natural aggregate, making them widely applied in construction [8]. However, the construction utilization of CW aggregate is limited due to its high water absorption; consequently, an effective way is needed to dispose of such CW waste [12,13]. CW has a higher embodied carbon (0.213 kg CO₂/kg) than natural aggregates (0.0075 kg CO₂/kg). Consequently, CW replacement for natural aggregates has limited environmental benefits compared to the partial replacement of Portland cement (0.912 kg CO₂/kg) [14,15]. Therefore, one option is to use the CW powder as a supplementary cementitious material (SCM) to reduce the environmental impact of construction [16].

Table 1 summarizes previous studies [17–25] of the use of ceramic wastes as SCM. These studies confirmed the pozzolanic activity of CW and identified the effects of using CW as a replacement for Portland cement on the physical and mechanical properties of mortar and concrete. O’Farrell et al. [26], Toledo Filho et al. [27], Zito et al. [28], and Pacheco-Torgal et al. [29] studied the effect of replacing up to 40% of Portland cement with CW, reporting a notable reduction in compressive strength at early ages, but only a minor decrease at later age.

Table 1. Previous studies.

Paper	Type of Ceramic Waste Used	% Replacement	Tests Performed	Main Findings
[17]	Ceramic block, mud-brick, and sanitary ware from the ceramic industry	24	Fratini test, XRD, FTIR, and non-evaporable water content. Chloride penetration, sulfate attack, and ASR.	All CWs show pozzolanic activity at 28 days, reduce the apparent chloride diffusion coefficient, perform well against the sulfate attack, and reduce the expansion caused by ASR.
[18]	Bricks powder generated from the ceramic industry.	5, 10, 15, 20	Physicochemical and mineralogical properties. Mechanical strengths and SEM for mortar.	Waste brick improves the grinding time and decreases the setting times. A 10% addition of CW increased mortar mechanical strengths at 90 days. Results confirmed the pozzolanic activity of CW.
[19]	Bricks powder generated from the ceramic industry.	10, 15, 20, 25, 30, 40	Pozzolanic properties. Compressive strength of concrete.	CW shows pozzolanic properties. Compressive strengths decrease with increasing CW content at early ages. CW < 20% slightly affects the strength.
[20]	Bricks powder generated from the ceramic industry	10, 20, 30, 40, 50	Compressive strength, toxicity characteristic of leaching, pozzolanic activity, XRD, and FTIR	Heavy metals leaching concentrations of waste brick were lower than the regulatory limits. At 28 days, the pozzolanic reaction began, reducing the amount of CH and increasing the densification. CW shows pozzolanic activity.
[21]	Ground calcined-clay brick.	10, 20, 30, 40	Stress–strain curves, pore size distribution, total porosity, sorptivity, and chloride penetration.	CW refined the pore structure and reduced macropores and total porosity. Reduction in modulus of elasticity and uniaxial compressive strength of mortars when the CW replacement was higher than 10%.
[22]	Glass, bricks, and tiles of red clay from the ceramic industry.	10, 20, 25, 30, 40	Mortar workability, mortar strength, and ASR.	CW replacements slightly decrease the fresh mortar consistency. From 28 to 90 days, compressive strength gain was higher for mortar with tile powders. SAI at 28 days > 0.75. Confirmation of the pozzolanic activity of CW, making their incorporation as cement mortars and concrete components feasible.
[23]	Ground clay roof tiles.	10, 20	Pozzolanic activity (lime consumption), compressive strength of mortar, and SEM.	CW has good pozzolanic properties; at an early age, the pozzolanic activity was higher than fly ash, although it was lower than silica fume. The morphologies of clay tile–PC pastes are similar to those of pastes containing other pozzolanic materials.
[24]	Sanitary ware from the ceramic industry and recycled fine aggregate from C&DW.	10, 20	Rheology and conduction calorimetry.	SW reduced shear yield stress and stunted the hydration reactions. C&DW had the opposite effect, raising yield stress and accelerating hydration kinetics. Cement particle hydration was modified depending on the type of CW: the reaction is accelerated by the inclusion of C&DW and stunted by SW.
[25]	Tile from the ceramic industry.	20, 30	SEM-EDX, XRD, and FTIR; laser granulometry, lime consumption, Fratini test, compressive strength, and the evolution of hydration (XRD and FTIR).	The compressive strength of blended cements was greater than 75% OPC at 28 days. CW < 30% does not significantly affect the compressive strength when the pozzolanic reaction contributes at later ages.

Masonry construction, which comprises different materials and typologies [30,31], is widely used in urban centers worldwide. In Spain, Portugal, and Latin America, traditional building features include reinforced concrete and ceramic walls as envelopes, resulting in a significant fraction of C&DW corresponding to the demolition of walls. For example,

in Madrid, Spain, more than half (54%) of C&DW consists of CW [32]. Similarly, in Bahía Blanca, Argentina, 31% of C&DW is attributed to the demolition of ceramic walls [33]. The waste from the demolition of ceramic walls comprises a mixture of ceramic and mortar, with proportions of approximately 56% ceramic and 44% masonry mortar by weight. This mortar is composed of sand, lime, and cement. Recycling these materials as SCM opens a promising new opportunity for managing C&DW.

As Table 1 shows, the previous studies used CW from the ceramic industry as SCM. For this reason, a new line of research is being explored around the use of wastes generated by demolition of ceramic block walls, since they are one of the primary sources of ceramic waste [34]. The present study introduces an innovation by analyzing the effects of finely ground recycled complete walls of ceramic blocks (including masonry mortars) as SCM on concrete's physical, mechanical, and transport mechanisms (water absorption and permeability). The replacement used was 25% by weight of cement. Studies of the evolution of the hydration of cement pastes support the described properties of the concrete.

2. Results and Discussions

2.1. Pozzolanicity and Hydration

Figure 1 shows the calorimetric curves (solid line) up to 48 h for OPC and 25CBW pastes. During the first minutes of hydration, the heat release rate was high due to the dissolution of clinker phases [35]. Next, the rate decreased drastically, leading to the recorded first minimum. In the case of the OPC sample, the first minimum was observed and recorded at approximately 125 min with a rate of 0.30 mW/g, while for the 25CBW sample, it occurred at 145 min, with a rate of 0.42 mW/g. Subsequently, the dormant period occurs, which is characterized by a low heat release rate in which mainly ionic exchanges occur [35]. It can be observed that this period was shorter for the 25CBW paste than for the OPC. This period is associated with the waste providing alkalinity (it contains CH from the masonry mortars); therefore, the pH necessary to trigger the continuation of the reactions is reached more quickly [36].

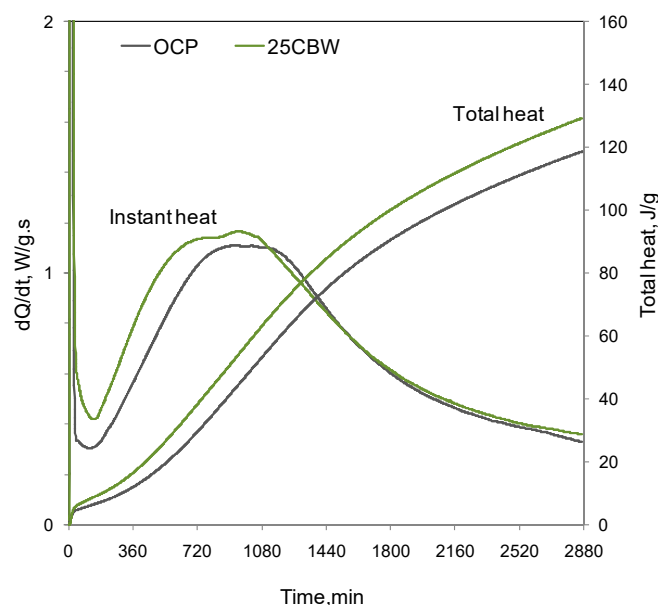


Figure 1. Heat liberation.

Next, the acceleration occurred due to the C_3S hydration achieving the second maximum [16]. The OPC paste reaches the second maximum at 920 min with a rate of 1.11 mW/g, while the 25CBW paste reaches the second maximum at 780 min with a rate of 1.14 mW/g. In the 25CBW paste, the reactions re-accelerated to reach the third maximum at 950 min with a rate of 1.16 mW/g. Finally, the hydration reactions decelerated, consequently decreasing the heat release rates.

In summary, dilution and stimulation effects were observed in the first hours of paste hydration due to incorporation of the CBW. The dilution effect was manifested by the delay in the first minimum in the 25CBW paste (20 min) concerning the OPC paste. The dilution resulted from incorporating CBW and increasing the effective water-to-cement ratio (w/c) (from 0.50 in the OPC paste to 0.66 in the 25CBW paste). The stimulation effect was manifested in the second maximum of the 25CBW paste ($\sim 2:20'$ before OPC paste) and the increase in its intensity concerning OPC paste. This effect was also manifested by the presence of the third maximum of the calorimetric curve of the 25CBW paste, showing the reactivity of the aluminum phase of the CBW. The stimulation of cement hydration was produced due to the filler effect, heterogeneous nucleation, and a large amount of free water being present in the system [37].

Figure 1 shows the total heat released during the first 48 h of hydration. It can be observed that the total heat released by the 25CBW paste (128 J/g) was higher than that of the OPC paste (118 J/g), evidencing the stimulation effect of the OPC due to the incorporation of CBW, despite the dilution.

Figure 2 shows the results of the Frattini test at different ages (2, 7, and 28 days) for the OPC and 25CBW samples. At 2 and 7 days, sample 25CBW was located above the CH solubility isotherm, as well as below and to the left of the OPC sample, with the decrease in $[\text{CaO}]$ (between 2 and 7 days) being lower for sample 25CBW than for OPC. This position shows the dilution effect that the CBW exerts on OPC, which is given by the decrease in $[\text{OH}^-]$ and $[\text{CaO}]$ of sample 25CBW concerning OPC. At 28 days, 25CBW paste showed a reduction in $[\text{CaO}]$, confirming the CBW's pozzolacinity, and an increase in $[\text{OH}^-]$ due to alkalis released by CBW. These results are in agreement with Asensio et al. 2016 [34]. This author indicates that the pozzolanic activity of the ceramic-based C&DW is directly related to the content of the ceramic material. In the existing literature [16–25], there is proven evidence of the pozzolanic activity of ceramic materials.

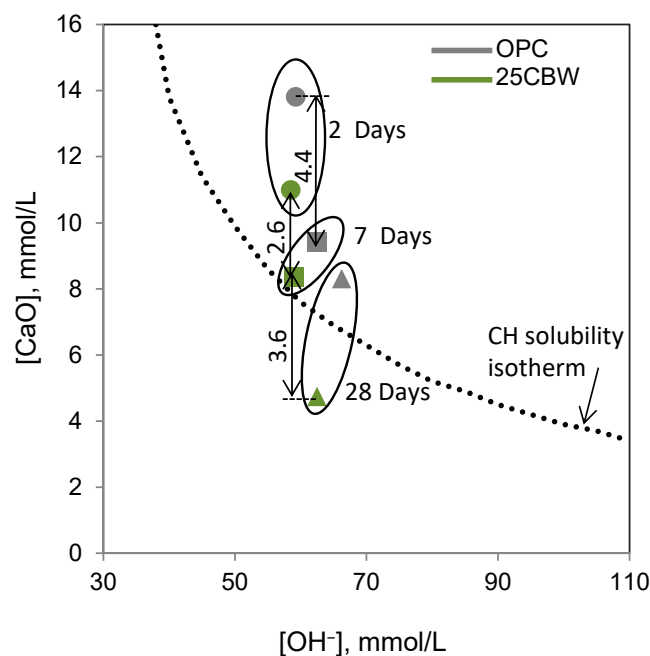


Figure 2. Frattini test results at 2, 7, and 28 days.

Figures 3 and 4 show the diffractograms and spectrograms of the OPC and 25CBW pastes at 2, 7, and 28 days of hydration. The OPC diffractograms (Figure 3a) show hydration progress, as the anhydrous cement compounds (C_3S , C_2S) decreased with age, while the hydrated phases evolved. At 2 days, ettringite (Et) and CH were observed as the main hydration products. The latter product was also detected in spectrograms (Figure 4a), where hydrated calcium silicate (C-S-H) was identified with a very intense band

in 970 cm^{-1} (Si_3SiO_4) [38]. CH was identified by the band at 3640 cm^{-1} [20], and Ett was identified by the band at 1120 cm^{-1} [39]. From days 7 to 28, the progress of the hydration of the silicates can be seen via two techniques: XRD, i.e., the intensity of the CH peaks, and FTIR, i.e., the sharpening of the 3640 cm^{-1} band of CH and 970 cm^{-1} band of C-S-H. The assigned bands to OH (3400 cm^{-1} and 1650 cm^{-1}) indicate the hydration progress [40].

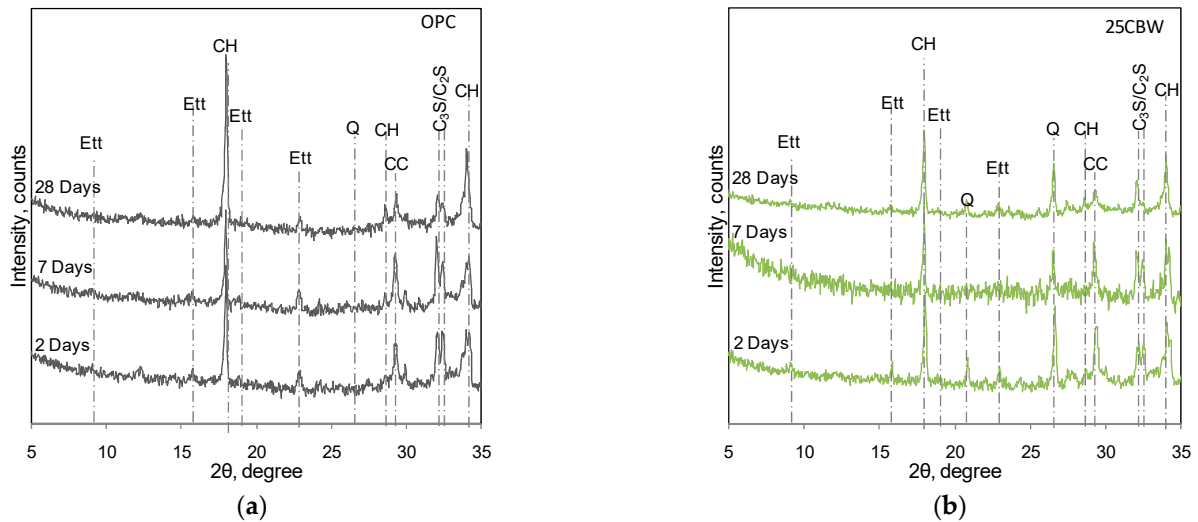


Figure 3. XRD patterns at 2, 7, and 28 days: (a) OPC; (b) 25CBW.

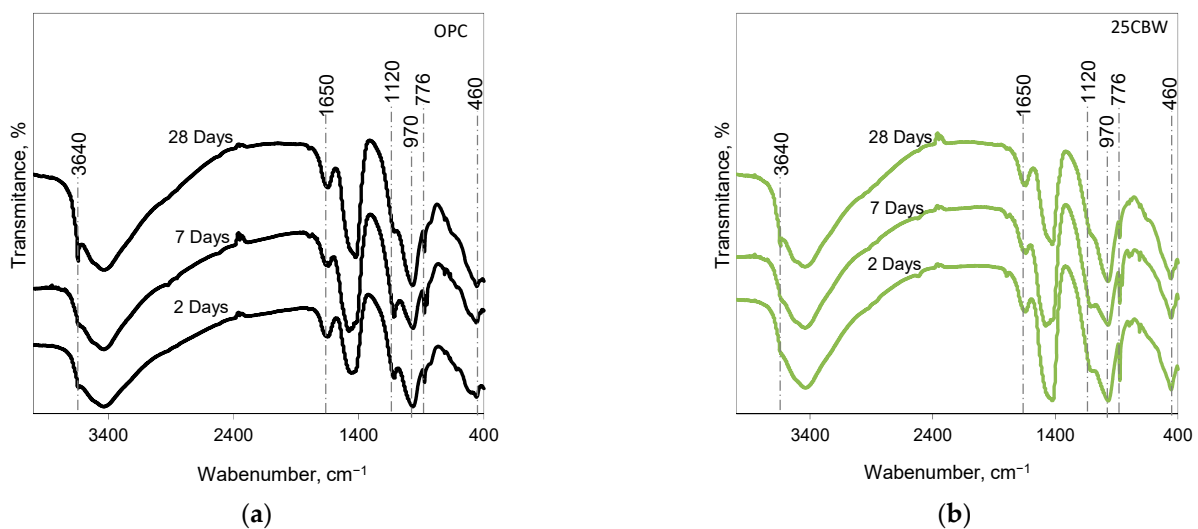


Figure 4. FTIR spectrum at 2, 7, and 28 days: (a) OPC; (b) 25CBW.

On the other hand, in the 25CBW paste (Figure 3b), the same compounds were detected via XRD as being in the OPC paste, in addition to the quartz (Q) coming from the CBW, and their evolution was similar, except for the intensity of the peaks assigned to CH, which decreased. Through FTIR (Figure 4b), the results found via XRD were confirmed, and it was also possible to observe the sharpening of the band at 970 cm^{-1} of the C-S-H. In line with the Frattini test results, we corroborated CH consumption by the pozzolanic reactions to provide more hydration products.

The amounts of non-evaporable water (W_n) at different ages (2, 7, and 28 days) for OPC and 25CBW pastes are reported in Table 2. As expected, the W_n content increases with increasing age for all pastes. The OPC paste exhibits a rapid growth in W_n content between 2 and 7 days, while the growth rate slows down at 28 days. At both 2 and 7 days, the W_n content of the 25CBW paste is higher than that of OPC, corresponding to the

proportion of OPC present in the 25CBW paste. However, at 28 days, the Wn content of the 25CBW paste reaches a level similar to that of OPC. These findings indicate that the CBW contributes to the Wn content at later ages, highlighting its pozzolanic activity. Moreover, these results align closely with the findings reported by Reig et al. [41], who observed significant strength gain as being provided by ceramic waste after 28 days of curing.

Table 2. Non-evaporable water (Wn).

Pastes	Wn, g/g		
	2 Days	7 Days	28 Days
OPC	0.132	0.178	0.199
25CBW	0.115	0.153	0.198

The mechanical compressive strength of the OPC mortar at 28 days was 39.48 MPa (B), while the 25CBW mortar’s compressive strength was 33.17 MPa (A). Therefore, an SAI ($A/B \times 100$) greater than 84% was obtained, indicating that CBW is an active pozzolan. The present data were also comparable to values reported by Zito et al. (2021) [17]. They observed pozzolanic activity, with SAI values ranging between 89.63 and 94.5% in mortars prepared with CW and cured for 28 days.

2.2. Fresh Properties, Mechanical Properties and Transport Mechanisms of Concrete

Figure 5 illustrates the bleeding curves of the concretes, which are represented by continuous lines. Incorporating CBW into the concrete reduces bleeding compared to ordinary Portland cement (OPC) concrete. Specifically, the bleeding rate of the 25% CBW concrete was approximately 47% lower than that of the OPC concrete, and the bleeding capacity was 68% lower. This reduction in the bleeding rate and capacity can be attributed to capillary pores being blocked by the CBW particles, which hindered water movement through the concrete. Additionally, the large specific external surface area (SEB) of CBW (as shown in Table 4) contributed to the decrease in free water content in the concrete, thereby reducing the bleeding capacity [42].

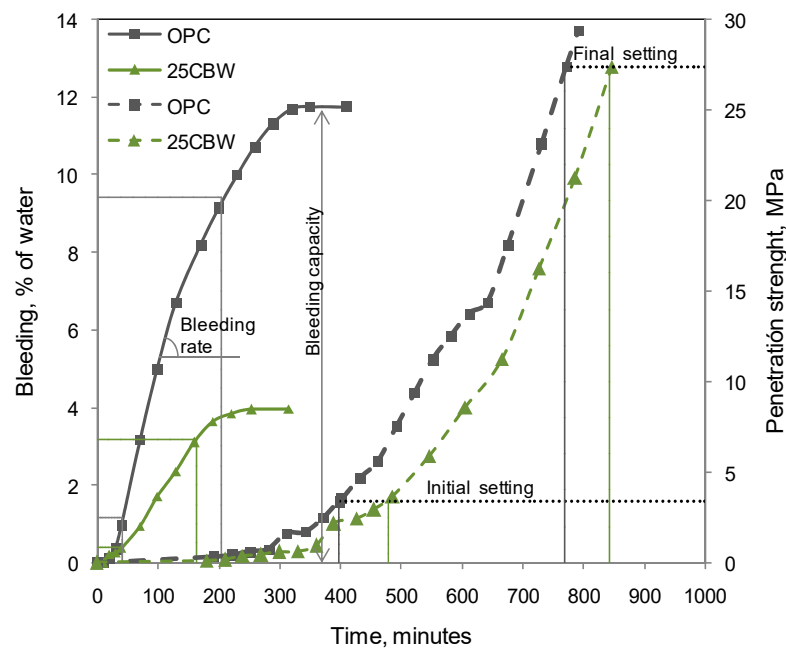


Figure 5. Bleeding and setting time of concretes.

Regarding the setting time of the concrete, as depicted by the dotted line in Figure 5, the OPC concrete exhibited an initial setting time of 395 min, while the 25% CBW concrete

had a longer initial setting time of 480 min. The final setting time for OPC was 770 min, whereas for the 25% CBW concrete, it was 845 min. The addition of CBW delayed both the beginning and the end of the setting time; however, the total setting time remained within the range of 365–375 min.

Figure 6 shows the evolution of the compressive and splitting tensile strengths for all concretes. The concrete strength increases over time, and the 25CBW concrete strength consistently falls below that of the OPC concrete at all ages. The relative compressive strength, which is represented by the dashed line, remains below 0.75 at 2 days, but surpasses 0.75 after 7 days. By 28 and 90 days, the 25% CBW concrete achieves a relative strength of 0.95. Conversely, the relative splitting tensile strength is below 0.75 at 2 days and remains comparable to the OPC concrete at 7 days. At 28 and 90 days, the 25% CBW concrete reaches a relative strength of 0.85.

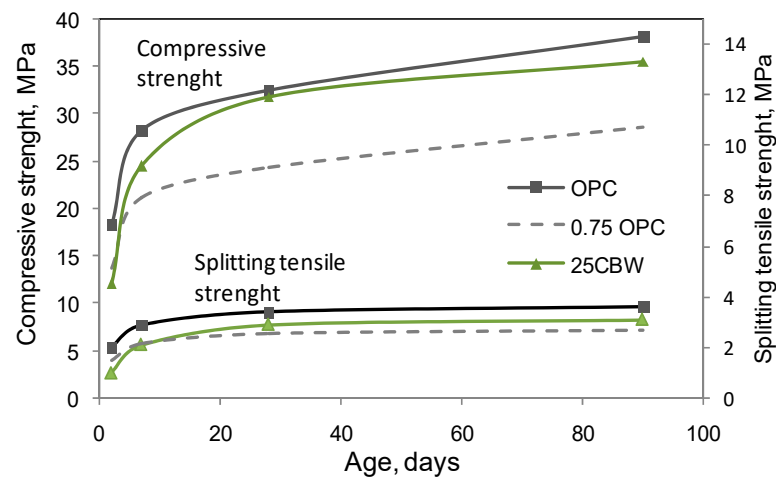


Figure 6. Compressive strength and splitting tensile strength of concretes.

Table 3 reports the elastic modulus of concretes that increased with age. For 25CBW concrete, the elastic modulus was lower than OPC concrete for up to 28 days. The relative elastic modulus was superior to 0.84 and 1.00 at 90 days.

Table 3. Concrete parameters.

Property		Concrete	
		OPC	25CBW
Elastic modulus, GPa	2 days	25.8	21.8
	7 days	31.0	26.6
	28 days	33.0	29.6
	90 days	40.7	40.8
Initial rate of water absorption, $S_1 \text{ g/m}^2 \cdot \text{s}^{1/2}$	2 days	45.0	24.8
	7 days	12.3	8.5
	28 days	8.5	6.7
Sorptivity capacity, g/m^2	2 days	5583	5273
	7 days	4288	4218
	28 days	4036	3518
Water penetration, mm	Average	19.5	20.6
	Maximum	26.0	31.7
	Minimum	12.0	9.0

In summary, the low strength values of 25CBW concrete (i.e., relative strength lower than 0.75) at 2 days were due to the dilution effect caused by the addition of CBW. The reduced clinker content increases the effective w/c ratio (from 0.5 for OPC concrete to 0.66 for 25CBW concrete), which could not be compensated by the higher hydration degree

of clinker phases [43]. At 7 days, the incipient pozzolanic reaction of CBW partially compensates for the dilution effect, reaching a relative strength greater than 0.75. Finally (at 28 and 90 days), the pozzolanic reaction generated secondary C-S-H that favored compressive strength development, reaching a relative compressive strength of >0.95 . These effects were also reflected in the modulus of elasticity, which, at 90 days, was slightly higher than in OPC concrete.

Table 3 reports the initial rate of water absorption (S1) and the sorptivity capacity (C) for both concretes measured after 2, 7, and 28 days of curing. S1 and C decreased for both concretes studied with increasing age. At 28 days, the sorptivity capacity (C) of the 25CBW concrete was 12% lower than that of the OPC concrete. It is worth mentioning that the secondary rate of water absorption (S2) calculated from 1 to 7 days was not reported due to the obtained linear regression having an R-squared value (R^2) of less than 0.98.

The improvement in capillary suction of concrete with CBW can be attributed to the physical and chemical processes that densify the concrete microstructure. Firstly, replacing clinker with CBW fills the voids, resulting in a denser and less interconnected pore structure. Secondly, the pozzolanic reaction and the continuous formation of secondary hydration contribute to an even denser microstructure [44].

Table 3 shows the water penetration depth in concrete at 28 days. The average water penetration of 25CBW concrete was only 5.6% higher than that of OPC concrete. These findings align with the sorptivity results, indicating that the presence of CBW has a limited impact on water penetration in concrete.

3. Materials and Methods

For this research, the material was obtained from demolition of a 30-year-old ceramic block wall (CBW), including masonry mortars. The Ordinary Portland Cement (OPC) chosen for comparison was equivalent to Type I cement, as per ASTM C150 [45].

The CBW samples were sourced from the demolition of a building in Olavarría, Buenos Aires, Argentina. Initially, the CBW was crushed until it could pass through a 4.75 mm sieve (#4). Subsequently, the crushed CBW was further ground in a ball mill until all particles could pass through a 75 μm sieve (#200). Finally, the particle size distribution was determined via laser granulometry (Malvern Masterziser, 2000). The original C&DW and the CBW after grinding are shown in Figure 7.



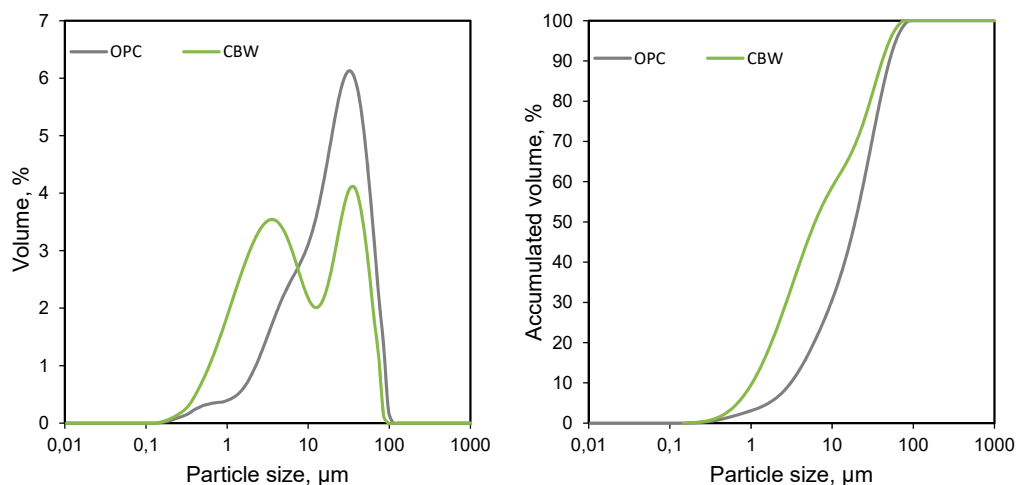
Figure 7. CBW grinding process.

Table 4 reported the physical properties and chemical composition of the OPC and CBW. For CBW, the sum of silica, alumina, and iron content exceeded the limit (70%) specified by the ASTM C618 standard [46]. Additionally, the CBW exhibited a higher loss of ignition than OPC, which was attributed to the decomposition of carbonates and hydrated phases in the masonry mortars. The density of the CBW was lower than that of OPC, but the specific surface area Blaine (SEB) was higher.

Table 4. The chemical composition and physical properties of the OPC and CBW.

Materials	OPC	CBW
Chemical composition, % by mass		
SiO ₂	20.50	62.36
Al ₂ O ₃	4.10	12.03
Fe ₂ O ₃	4.70	4.19
CaO	63.60	8.36
MgO	0.70	0.93
SO ₃	2.50	0.15
K ₂ O	1.20	3.34
Na ₂ O	<0.03	1.44
TiO ₂	-	0.56
Loss on ignition	2.40	6.01
SiO ₂ + Al ₂ O ₃ + Fe ₂ O ₃		74.39
Equivalent alkalis (Na ₂ O + 0.658 K ₂ O), %		3.63
Physical properties		
Density, g/cm ³	3.12	2.58
SEB, m ² /kg	370	660
Particle size distribution μm		
D ₁₀	3.30	1.11
D ₅₀	20.51	6.58
D ₉₀	86.36	44.23

Figure 8 shows the particle size distribution of OPC and CBW. The particle size distribution of the CBW shows two maximums (around 3.8 and 38 μm) due to the mineral mixture present in the masonry mortars (siliceous and calcareous nature). The particle size distribution of OPC presents a prominent peak at 30.6 μm. These results agree with the parameters D₁₀, D₅₀, and D₉₀, as shown in Table 4.

**Figure 8.** Particle size distribution curve of OPC and CBW.

The mineralogical composition of the Portland clinker, as provided by the manufacturer, was described as follows (% by mass): 63.60 C₃S, 15.10 C₂S, 2.80 C₃A, and 14.30 C₄AF. Additionally, OPC contained gypsum and limestone as minor components. The mineralogical composition of CBW was obtained via X-ray diffraction (XRD, (Figure 9a) using a Philips PW3710 diffractometer operating with Cu-K α radiation at 40 kV and 20 mA. The mineralogical composition of CBW included quartz (SiO₂), anorthite (CaAl₂Si₂O₈), hematite (Fe₂O₃), calcite (CaCO₃), and a small diffuse dome in the 18 to 30° 2 θ range, indicating the presence of amorphous phases [47,48]. The FTIR spectra (Figure 9b) were performed on Nicolet Magna 500 using the KBr technique, confirming the phases determined using XRD. Quartz was identified by bands around 796 and 776 cm⁻¹, which was characteristic of the

symmetric stretching of the Si-O bond [49]. Anorthite was identified through the band at 543 cm^{-1} , which was characteristic of the vibration of the AlO_6 group [50,51]. The band at 1434 cm^{-1} corresponded to calcite, which was associated with the asymmetric vibration of the O-C-O bond. The band at 1075 cm^{-1} was related to asymmetric Si-O-Si or Si-O-Al stretching of amorphous aluminosilicates [52,53]. The band at 460 cm^{-1} corresponded to the bending of the Si-O-Si bond of quartz and the amorphous aluminosilicate phase [48]. Iron minerals, which were detected via XRD, were challenging to identify based on their FTIR spectra due to overlapping silicates [25].

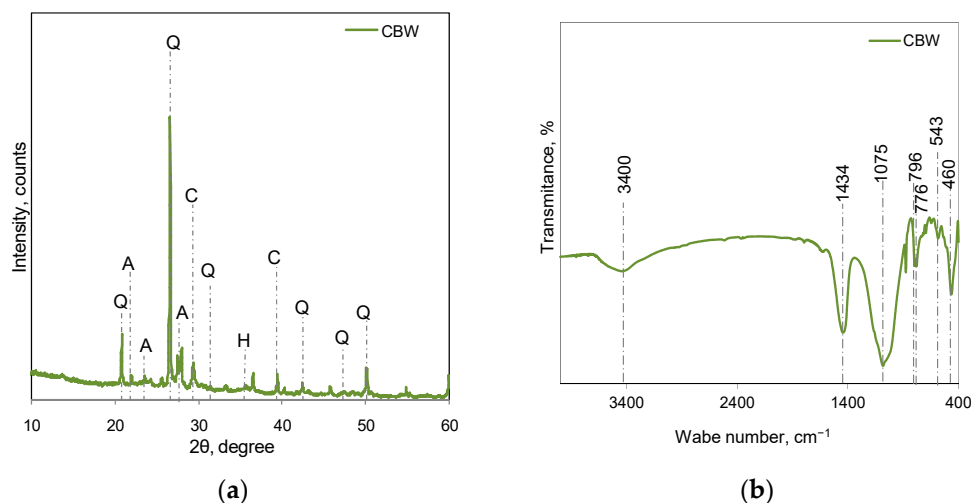


Figure 9. (a) XRD pattern of CBW. Q: quartz; A: anorthite; H: hematite; C: calcite. (b) FTIR spectrum for CBW.

The tests were carried out on two samples OPC (100% OCP) and 25CBW (75% OCP + 25% CBW, by weight). The replacement percentage used was based on the recommendation of EN 450-1:2013 for use of fly ash as a replacement of Portland cement in concrete [54]. The experimental program was divided into two parts. In the first part, the pozzolanic activity of the CBW was checked, and the hydration of the OPC and the 25CBW pastes were monitored. The behavior of fresh and hardened concrete (mechanical strength and transport mechanisms) was studied in the second part.

3.1. Pozzolanicity and Hydration

The heat release rate in paste with a water cementitious material ratio (w/cm) of 0.5 was measured using an isothermal conduction calorimeter operating at $20\text{ }^{\circ}\text{C}$ during an early-age period ($<48\text{ h}$). The total heat released was also calculated by integrating the area under the heat-released rate curve over time.

At 2, 7, and 28 days, the Frattini test determined the pozzolanic activity (EN196-5, [55]). Positive pozzolanic activity was indicated when the test points fall below the solubility isotherm of calcium hydroxide (CH) at $40\text{ }^{\circ}\text{C}$.

XRD and FTIR were employed to identify the hydration phases in blended cement pastes ($w/cm = 0.50$) at 2, 7 and 28 days. The equipment and analysis parameters mentioned previously were used for these analyses. The chemically combined water (W_n), which indicates the amount of hydrated cement, was determined by following the procedure proposed by Powers [56]. W_n was obtained in pastes ($w/cm = 0.5$) by measuring the mass loss between 100 and $950\text{ }^{\circ}\text{C}$.

Finally, the strength activity index ($\text{SAI} = A/B \times 100$) was calculated as the ratio of the compressive strength of 25CBW mortar (A) to the strength of the OPC mortar (B) at 28 days. The pozzolan is active when SAI is greater than 75% at 28 days (ASTM C 618 [46] and EN 450-1 [54]). For this purpose, RILEM mortar prisms ($40 \times 40 \times 160\text{ mm}^3$) were prepared using standard sand (1:3) and $w/cm = 0.50$.

3.2. Fresh Properties, Mechanical Properties, and Transport Mechanisms of Concretes

The concretes were prepared with a cementitious material content of 350 kg/m^3 and a water-to-cementitious material ratio (w/cm) of 0.50. The coarse aggregate used was crushed granite sourced from Olavarría, Buenos Aires. It had a density of 2.70 kg/dm^3 , a maximum nominal size of 16 mm, and bulk densities in loose and compacted conditions of 1430 kg/m^3 and 1560 kg/m^3 , respectively. The coarse aggregate content was 1050 kg/m^3 for both concretes, maintaining an acceptable aggregate/total aggregate ratio of 0.43. Fine aggregate was obtained from the Paraná River in Argentina with a 2.67 kg/dm^3 density and a fineness modulus of 2.35. To compensate for the density differences between OPC and 25CBW, the fine aggregate content was adjusted to 807 kg/m^3 for OPC concrete and 806.5 kg/m^3 for 25CBW concrete.

A polycarboxylate-based superplasticizer (SP) (BASF, Trostberg, Germany) was used to guarantee the proper workability of the fresh concrete. The dosage was adjusted to obtain concretes within consistency S2 according to DIN-EN 206 [57]. For OPC concrete, the SP dosage used was 0.24%, which was measured by the weight of the cementitious material; for 25CBW, it was almost unnecessary to increase the dosage (0.25%). In fresh concrete, the setting time was determined according to the ASTM 403 [58] standard, and the bleeding capacity and bleeding rate were calculated according to the ASTM C232, Method A [59] standard. The mechanical properties determined were as follows: compressive strength (ASTM C39, [60]), splitting tensile strength (ASTM C496, [61]), and static modulus of elasticity (ASTM C469, [62]) on cylinders at 2, 7, 28, and 90 days. Six samples were used for each of the determinations. The relative strength was calculated as the ratio of the strength of OPC to 25CBW at the same age.

The water transport properties of the concrete were investigated through capillary absorption (sorptivity) using the ASTM C 1585 standard [63]) and water penetration under pressure using the DIN EN 12390-8 standard [64]. Water sorptivity was determined by testing cylinders with diameters of 100 mm and heights of 50 mm, which were cured for 2, 7, and 28 days. Water penetration under pressure was measured via 150 mm cubes cured for 28 days using three specimens.

4. Conclusions

Considering the test results obtained in this study and the aim of recycling ceramic waste from construction and demolition waste (complete walls of ceramic blocks including masonry mortars), the following conclusions can be drawn.

The CBW stimulated the hydration of the cement paste physically (filler effect) at early ages and chemically (pozzolanic reaction) at later ages. The hydration products revealed that the hydration mechanisms of the cement with the CBW were similar to those of the pure cement.

The concrete with CBW presented similar behavior in terms of uniformity, finish, slump, and having lower bleeding rate. Mechanical properties at early ages showed that physical stimulation did not compensate for the dilution effect caused by CBW. Nonetheless, at late ages, the pozzolanic activity contributed to the complete compensation of the dilution effect. On the other hand, the sorptivity capacity and initial rate of water absorption in the concrete with CBW were lower than in the reference concrete, reflecting the microstructural densification via the physical–chemical actions produced by the CBW, thus resulting in an equivalent permeability.

Recycling base ceramics wastes as SCM contributes to the transition towards a circular economy model by reducing C&DW.

5. Limitations and Recommendations for Further Studies

This study was limited to testing only one source of ceramic block wall. Variations in the types of ceramic and mortar in the demolished wall and their proportions may affect the test results. In addition, the Portland cement replacement of 25% by weight was recommended for EN 450 and fly ash. This percentage is not necessarily the optimum

replacement percentage for CBW. Future studies are needed to test different sources of CBW and different percentages of Portland cement replacement to verify the results of the current study.

Author Contributions: Investigation, conceptualization, methodology, and writing—original draft preparation, S.V.Z.; supervision, review, and editing, V.F.R. and E.F.I. All authors have read and agreed to the published version of the manuscript.

Funding: This work was supported by the Comisión de Investigaciones Científicas de la Provincia de Buenos Aires (CICPBA) and Consejo Nacional de Investigaciones Científicas y Técnicas (CONICET) (PIO-04) and the Universidad Nacional del Centro de la Provincia de Buenos Aires (Project E02/122).

Data Availability Statement: All data, models, and code generated or used during the study appears in the published article.

Acknowledgments: The researchers acknowledge the support provided by the CICPBA and CONICET (PIO-004), as well as by the Universidad Nacional del Centro de la Provincia de Buenos Aires (Project E02/122).

Conflicts of Interest: The authors declare no conflict of interest.

References

1. Tam, V.W.; Tam, C.M. A review on the viable technology for construction waste recycling. *Resour. Conserv. Recycl.* **2006**, *47*, 209–221. [CrossRef]
2. Rosa, J.; Pastó, E. Gestión de escombros y otros residuos de la construcción. *Rev. Ambiente* **2004**, *24*, 53–56.
3. Organisation for Economic Co-Operation and Development (OECD). *Towards a More Resource-Efficient and Circular Economy: The Role of the G20*; OECD: Paris, France, 2021.
4. López Ruiz, L.A.; Roca Ramón, X.; Gassó Domingo, S. Economía circular en el sector de los residuos de construcción y demolición: Análisis de iniciativas en España. In Proceedings of the 24th International Congress on Project Management and Engineering, Alcoy, Spain, 7–9 July 2020; pp. 1320–1334.
5. Akhtar, A.; Sarmah, A.K. Construction and demolition waste generation and properties of recycled aggregate concrete: A global perspective. *J. Clean. Prod.* **2018**, *186*, 262–281. [CrossRef]
6. Seror, N.; Portnov, B.A. Estimating the effectiveness of different environmental law enforcement policies on illegal C&D waste dumping in Israel. *Waste Manag.* **2020**, *102*, 241–248. [CrossRef]
7. Xiao, J.; Ma, Z.; Ding, T. Reclamation chain of waste concrete: A case study of Shanghai. *Waste Manag.* **2016**, *48*, 334–343. [CrossRef] [PubMed]
8. Yang, D.; Liu, M.; Ma, Z. Properties of the foam concrete containing waste brick powder derived from construction and demolition waste. *J. Build. Eng.* **2020**, *32*, 101509. [CrossRef]
9. Shooshtarian, S.; Caldera, S.; Maqsood, T.; Ryley, T. Using recycled construction and demolition waste products: A review of stakeholders' perceptions, decisions, and motivations. *Recycling* **2020**, *5*, 31. [CrossRef]
10. Guo, H.; Shi, C.; Guan, X.; Zhu, J.; Ding, Y.; Ling, T.C.; Wang, Y. Durability of recycled aggregate concrete—A review. *Cem. Concr. Compos.* **2018**, *89*, 251–259. [CrossRef]
11. Liang, C.; Ma, H.; Pan, Y.; Ma, Z.; Duan, Z.; He, Z. Chloride permeability and the caused steel corrosion in the concrete with carbonated recycled aggregate. *Constr. Build. Mater.* **2019**, *218*, 506–518. [CrossRef]
12. Liang, C.; Pan, B.; Ma, Z.; He, Z.; Duan, Z. Utilization of CO₂ curing to enhance the properties of recycled aggregate and prepared concrete: A review. *Cem. Concr. Compos.* **2020**, *105*, 103446. [CrossRef]
13. Yang, J.; Du, Q.; Bao, Y. Concrete with recycled concrete aggregate and crushed clay bricks. *Constr. Build. Mater.* **2011**, *25*, 1935–1945. [CrossRef]
14. Pradhan, S.; Tiwari, B.R.; Kumar, S.; Barai, S.V. Comparative LCA of recycled and natural aggregate concrete using particle packing method and conventional method of design mix. *J. Clean. Prod.* **2019**, *228*, 679–691. [CrossRef]
15. ICE. Data Base Embodied Carbon Model of Cement, Mortar and Concrete. Available online: <http://www.circularecology.com/embodied-energy-and-carbon-footprint-database.html> (accessed on 1 January 2022).
16. Rahhal, V.F.; Trezza, M.A.; Tironi, A.; Castellano, C.C.; Pavlíková, M.; Pokorný, J.; Pavlík, Z. Complex characterization and behavior of waste fired brick powder-portland cement system. *Materials* **2019**, *12*, 1650. [CrossRef] [PubMed]
17. Zito, S.V.; Cordoba, G.P.; Irassar, E.F.; Rahhal, V.F. Durability of eco-friendly blended cements incorporating ceramic waste from different sources. *J. Sustain. Cem.* **2021**, *12*, 13–23. [CrossRef]
18. Naceri, A.; Hamina, M.C. Use of waste brick as a partial replacement of cement in mortar. *Waste Manag.* **2019**, *29*, 2378–2384. [CrossRef]
19. Heidari, A.; Hasanpour, B. Effects of waste bricks powder of gachsaran, B. company as a pozzolanic material in concrete. *Asian J. Civ. Eng.* **2013**, *14*, 755–763.

20. Lin, K.L.; Wu, H.H.; Shie, J.L.; Hwang, C.L.; Cheng, A. Recycling waste brick from construction and demolition of buildings as pozzolanic materials. *Waste Manag. Res.* **2010**, *28*, 653–659. [[CrossRef](#)] [[PubMed](#)]
21. Gonçalves, J.P.; Tavares, L.M.; Toledo Filho, R.D.; Fairbairn, E.M.R. Performance evaluation of cement mortars modified with metakaolin or ground brick. *Constr. Build. Mater.* **2009**, *23*, 1971–1979. [[CrossRef](#)]
22. Pereira-de-Oliveira, L.A.; Castro-Gomes, J.P.; Santos, P.M.S. The potential pozzolanic activity of glass and red-clay ceramic waste as cement mortars components. *Constr. Build. Mater.* **2012**, *31*, 197–203. [[CrossRef](#)]
23. Sánchez de Rojas, M.I.; Marin, F.; Rivera, J.; Frías, M. Morphology and properties in blended cements with ceramic wastes as a pozzolanic material. *J. Am. Ceram. Soc.* **2006**, *89*, 3701–3705. [[CrossRef](#)]
24. Medina, C.; Banfill, P.F.G.; De Rojas, M.S.; Frías, M. Rheological and calorimetric behaviour of cements blended with containing ceramic sanitary ware and construction/demolition waste. *Constr. Build. Mater.* **2013**, *40*, 822–831. [[CrossRef](#)]
25. Lavat, A.E.; Trezza, M.A.; Poggi, M. Characterization of ceramic roof tile wastes as pozzolanic admixture. *Waste Manag.* **2009**, *29*, 1666–1674. [[CrossRef](#)] [[PubMed](#)]
26. O’Farrell, M.; Sabir, B.B.; Wild, S. Strength and chemical resistance of mortars containing brick manufacturing clays subjected to different treatments. *Cem. Concr. Compos.* **2006**, *28*, 790–799. [[CrossRef](#)]
27. Toledo Filho, R.D.; Gonçalves, J.P.; Americano, B.B.; Fairbairn, E.M.R. Potential for use of crushed waste calcined-clay brick as a supplementary cementitious material in Brazil. *Cem. Concr. Res.* **2007**, *37*, 1357–1365. [[CrossRef](#)]
28. Zito, S.V.; Irassar, E.F.; Rahhal, V.F. Management of sanitary ware wastes as supplementary cementing materials in concretes. *J. Sustain. Cem.* **2020**, *9*, 35–49. [[CrossRef](#)]
29. Pacheco-Torgal, F.; Jalali, S. Reusing ceramic wastes in concrete. *Constr. Build. Mater.* **2010**, *24*, 832–838. [[CrossRef](#)]
30. Angiolilli, M.; Gregori, A.; Vailati, M. Lime-Based Mortar Reinforced by Randomly Oriented Short Fibers for the Retrofitting of the Historical Masonry Structure. *Materials* **2020**, *13*, 3462. [[CrossRef](#)]
31. Vailati, M.; Mercuri, M.; Angiolilli, M.; Gregori, A. Natural-Fibrous Lime-Based Mortar for the Rapid Retrofitting of Heritage Masonry Buildings. *Fibers* **2021**, *9*, 68. [[CrossRef](#)]
32. Santos Jiménez, M.D.R. Reciclaje de Residuos de Construcción y Demolición (RCD) de Tipo Cerámico para Nuevos Materiales de Construcción Sostenibles. Ph.D. Dissertation, E.T.S. de Edificación (UPM), Madrid, Spain, 2018. [[CrossRef](#)]
33. Moro, J.M.; Meneses, R.S.; Ortega, N.F.; Aveldaño, R.R. Generación de Desechos de Hormigón y su Utilización como Agregado Grueso en Nuevos Hormigones. In Proceedings of the ISEU2010—Congreso de Ingeniería Sustentable y Ecología Urbana, Buenos Aires, Argentina, 13–15 October 2010.
34. Asensio, E.; Medina, C.; Frías, M.; de Rojas, M.I.S. Characterization of ceramic-based construction and demolition waste: Use as pozzolan in cements. *J. Am. Ceram. Soc.* **2016**, *99*, 4121–4127. [[CrossRef](#)]
35. de Matos, P.R.; Sakata, R.D.; Ongheero, L.; Uliano, V.G.; de Brito, J.; Campos, C.E.; Gleize, P.J. Utilization of ceramic tile demolition waste as supplementary cementitious material: An early-age investigation. *J. Build. Eng.* **2021**, *38*, 102187. [[CrossRef](#)]
36. Rahhal, V.; Talero, R. Calorimetry of Portland cement with metakaolins, quartz and gypsum additions. *J. Therm. Anal. Calorim.* **2008**, *91*, 825–834. [[CrossRef](#)]
37. Zhang, C.; Wang, A.; Tang, M.; Liu, X. The filling role of pozzolanic material. *Cem. Concr. Res.* **1996**, *26*, 943–947. [[CrossRef](#)]
38. Yu, P.; Kirkpatrick, R.J.; Poe, B.; McMillan, F.; Cong, X. Structure of calcium silicate hydrate (C-S-H): Near-, Mid-, and Far-infrared spectroscopy. *J. Am. Ceram. Soc.* **2004**, *82*, 742–748. [[CrossRef](#)]
39. de Lucas, E.A.; Medina, C.; Frías, M.; de Rojas, M.I.S. Clay-based construction and demolition waste as a pozzolanic addition in blended cements, Effect on sulfate resistance. *Constr. Build. Mater.* **2016**, *127*, 950–958. [[CrossRef](#)]
40. Trezza, M. Estudio de las Posibles Alteraciones en el Comportamiento del Cemento Portland por Incorporación de Impurezas (Óxidos y Sales Inorgánicas) Durante el Proceso de Clinkerización. Master’s Thesis, Universidad Nacional del Centro de la Provincia de Buenos Aires, Buenos Aires, Argentina, 1998.
41. Reig, L.; Soriano, L.; Borrachero, M.V.; Monzó, J.M.; Payá, J. Potential use of ceramic sanitary ware waste as pozzolanic material. *Boletín Soc. Española Cerám. Vidr.* **2022**, *61*, 611–621. [[CrossRef](#)]
42. Thienel, K.C.; Beuntner, N. Effects of calcined clay as low carbon cementing materials on the properties of concrete. In *Concrete in the Low Carbon Era*; Jones, M.R., Newlands, M.D., Halliday, J.E., Eds.; University of Dundee: Dundee, UK, 2012; pp. 504–518.
43. Cyr, M.; Lawrence, P.; Ringot, E. Efficiency of mineral admixtures in mortars: Quantification of the physical and chemical effects of fine admixtures in relation with compressive strength. *Cem. Concr. Res.* **2006**, *36*, 264–277. [[CrossRef](#)]
44. Beuntner, N.; Kustermann, A.; Thienel, K.C. Pozzolanic potential of calcined clay in high-performance concrete. In Proceedings of the International Conference on Sustainable Materials, Systems and Structures (SMSS 2019) New Generation of Con-Struction Materials, Rovinj, Croatia, 20–22 March 2019; pp. 20–22.
45. ASTM C150/C150M-20; Standard Specification for Portland Cement. ASTM International: Singapore, 2021.
46. ASTM C618-19; Standard Specification for Coal Fly Ash and Raw or Calcined Natural Pozzolan for Use in Concrete. ASTM International: Singapore, 2022.
47. Pitarch, A.M.; Reig, L.; Tomás, A.E.; Forcada, G.; Soriano, L.; Borrachero, M.V.; Monzó, J.M. Pozzolanic activity of tiles, bricks and ceramic sanitary-ware in ecofriendly Portland blended cements. *J. Clean. Prod.* **2021**, *279*, 123713. [[CrossRef](#)]
48. Chakchouk, A.; Trifi, L.; Samet, B.; Bouaziz, S. Formulation of blended cement: Effect of process variables on clay pozzolanic activity. *Constr. Build. Mater.* **2009**, *23*, 1365–1373. [[CrossRef](#)]

49. Puligilla, S.; Mondal, P. Co-existence of aluminosilicate and calcium silicate gel characterized through selective dissolution and FTIR spectral subtraction. *Cem. Concr. Res.* **2015**, *70*, 39–49. [[CrossRef](#)]
50. Magi, M.; Lippmaa, E.; Samoson, A.; Engelhardt, G.; Grimmer, A.R. Solid-state high-resolution silicon-29 chemical shifts in silicates. *J. Phys. Chem.* **1984**, *88*, 1518–1522. [[CrossRef](#)]
51. Nampi, P.P.; Moothetty, P.; Berry, F.J.; Mortimer, M.; Warriar, K.G. Aluminosilicates with varying alumina–silica ratios: Synthesis via a hybrid sol–gel route and structural characterisation. *Dalton Trans.* **2010**, *39*, 5101–5107. [[CrossRef](#)]
52. Padmaja, P.; Anilkumar, G.M.; Mukundan, P.; Aruldas, G.; Warriar, K.G.K. Characterisation of stoichiometric sol–gel mullite by Fourier transform infrared spectroscopy. *Int. J. Inorg. Mater.* **2001**, *3*, 693–698. [[CrossRef](#)]
53. Popa, M.; Kakihana, M.; Yoshimura, M.; Calderón-Moreno, J.M. Zircon formation from amorphous powder and melt in the silicarich region of the alumina–silica–zirconia system. *J. Non-Cryst.* **2006**, *352*, 5663–5669. [[CrossRef](#)]
54. *UNE-EN 450-1:2013*; Fly Ash for Concrete—Part 1: Definition, Specifications and Conformity Criteria. European Standard: Brussels, Belgium, 2013.
55. *UNE-EN 196-5*; Methods of Testing Cement. Pozzolanicity Test for Pozzolanic Cement. British Standard Institution: London, UK, 2011.
56. Powers, T.C. The non-evaporable water content of hardened Portland cement paste. *ASTM Bull.* **1949**, *158*, 68–75.
57. *DIN EN 206*; Concrete—Specification, Performance, Production and Conformity. DIN (Deutsches Institut für Normung): Berlin, Germany, 2013.
58. *ASTM C403*; Standard Test Method for Time of Setting of Concrete Mixtures by Penetration Resistance. ASTM International: Singapore, 2017.
59. *ASTM C232/C232M-20*; Standard Test Method for Bleeding of Concrete. ASTM International: Singapore, 2019.
60. *ASTM C39/C39M-21*; Standard Test Method for Compressive Strength of Cylindrical Concrete Specimens. ASTM International: Singapore, 2021.
61. *ASTM C496/C496M-17*; Standard Test Method for Splitting Tensile Strength of Cylindrical Concrete Specimens. ASTM International: Singapore, 2017.
62. *ASTM C469/C469M*; Standard Test Method for Static Modulus of Elasticity and Poisson’s Ratio of Concrete in Compression. ASTM International: Singapore, 2014.
63. *ASTM C1585-20*; Standard Test Method for Measurement of Rate of Absorption of Water by Hydraulic-Cement Concretes. ASTM International: Singapore, 2020.
64. *DIN EN 12390-8-2019*; Testing Hardened Concrete—Part 8: Depth of Penetration of Water under Pressure. DIN (Deutsches Institut für Normung): Berlin, Germany, 2019.

Disclaimer/Publisher’s Note: The statements, opinions and data contained in all publications are solely those of the individual author(s) and contributor(s) and not of MDPI and/or the editor(s). MDPI and/or the editor(s) disclaim responsibility for any injury to people or property resulting from any ideas, methods, instructions or products referred to in the content.